Electronic Supplementary Material (ESI) for Materials Chemistry Frontiers.

Supporting Information

Engineering of anchor sites and metal-support interactions to synthesize high loading and stable sub-nanocluster catalysts

Di Wu [a], Dan Zhang [a, b], Zuochao Wang [a], Jixiang Xu [a], Xilei Chen [b], Jianping Lai *[, a] and Lei Wang *[,a,b]

[a] Key Laboratory of Eco-chemical Engineering, Taishan scholar advantage and characteristic discipline team of Eco-chemical process and technology, College of Chemistry and Molecular Engineering, Qingdao University of Science and Technology, Qingdao 266042, P. R. China

[b] Shandong Engineering Research Center for Marine Environment Corrosion and Safety Protection, College of Environment and Safety Engineering, Qingdao University of Science and Technology, Qingdao 266042, P. R. China

Experimental

Preparation of Pt/KB-O_S.

First, 10 mg KB powder, 15 mg K_2PtCl_6 and 5 mg sucrose were ground in a mortar for 30 min until mixed evenly, and then transferred to a quartz bottle. Then placed in a household microwave oven and reacted for 40 s with a power of 700 W. The obtained sample was denoted as $Pt_{0.6}$/KB-O_{S5}-40. What's more, Pt_x/KB-O_{S5}-40 samples with different amount of Pt added were synthesized by the same method except for changing the addition amount of Pt precursor (x=0.4, 0.6, 0.8, which means added 40%, 60% and 80% Pt precursor) By adjusting the type and amount of functional group precursor (y = S5, S20, M5, T5, F5, C5, where S is sucrose, M is melamine, T is thiourea, F is fructose and C is cellulose.), $Pt_{0.6}$/KB-O_{F5}-40, $Pt_{0.6}$/KB-O_{S5}-40, $Pt_{0.6}$/KB-O_{C5}-40, $Pt_{0.6}$/KB-O_{M5}-40, $Pt_{0.6}$/KB-O_{T5}-40 were obtained. The catalyst when sucrose is added at 0 is denoted $Pt_{0.6}$/KB-40. By adjusting the reaction time (20 s, 40 s and 60 s), $Pt_{0.6}$/KB-O_{S5}-20, $Pt_{0.6}$/KB-O_{S5}-40 and $Pt_{0.6}$/KB-O_{S5}-60 were obtained.

Preparation of $Pt_{0.6}$/CNT-O_{S5}-40 and $Pt_{0.6}$/rGO-O_{S5}-40.

First, 10 mg of MWCNT, 15 mg K_2PtCl_6 and 5 mg sucrose were ground in a mortar for 30 min until the mixture was evenly mixed. Then the mixture was transferred to a quartz bottle and reacted for 40 s with a power of 700 W. The material obtained was named as $Pt_{0.6}$/CNT-O_{S5}-40. $Pt_{0.6}$/rGO-O_{S5}-40 was synthesized by the same method except for changing the MWCNT to rGO.

Preparation of $Pd_{0.6}$/KB-O_{S5}-40 and $Ru_{0.6}$/KB-O_{S5}-40.

The synthesis method of $Pd_{0.6}$/KB-O_{S5}-40 and $Ru_{0.6}$/KB-O_{S5}-40 is the same as that of $Pt_{0.6}$/KB-O_{S5}-40, except that $PdCl_2$ and $RuCl_3$ replace K_2PtCl_6 respectively.

Electrochemical measurements.

Electrochemical characterization was carried out in a conventional three-electrode cell of a CHI-760E Electrochemical Workstation (Shanghai Chenhua Instrument Corporation, China) at room temperature. Ag/AgCl electrode and carbon rod were used as reference electrode and counter electrode respectively. All potentials were calibrated *vs* reversible hydrogen electrode (RHE) using the equation:

$$E_{RHE} = E_{Ag/AgCl} + 0.059\ pH + E^0_{Ag/AgCl}$$

Where E_{RHE} is the potential *vs*. RHE, $E_{Ag/AgCl}$ is the experimentally measured potential against the Ag/AgCl reference electrode, and $E^0_{Ag/AgCl}$ is the standard potential of Ag/AgCl at 25 ℃ (0.199 V).

The glassy carbon electrode (GCE, diameter: 3 mm, area: 0.07065 cm^2) was used as the working electrode. Catalyst ink was prepared by suspending 5 mg of catalyst powder in a 1 mL solution consisting of 5 wt% Nafion and ethanol (v: v=1:100). The catalyst ink obtained was supersonic treated for 30 minutes in room temperature in order to disperse evenly. Prior to dipping into the ink, the GCE was polished by Al_2O_3 powder to clean the surface. In a N_2-saturated 0.5 M H_2SO_4 solution, Linear sweep voltammetry (LSV) was carried out at a sweep rate of 5 mV s^{-1}. All catalysts need to be cyclic voltammetry (CV) activated before LSV testing. All polarization curves were corrected for 95% iR. The durability test was in 0.5 M H_2SO_4 solution using chronoamperometry. The ECSA can be derived using the formula: ECSA = S_{geo} *C_{dl}/C_s via C_{dl}, wherein, C_s is the specific electrochemical double layer capacitance, its value in acidic environments is 0.040 mF cm^{-2}, and S is the geometric surface area of the working electrode. The electrochemical impedance spectroscopy (EIS) measurement was performed over a frequency range of 0.1 Hz to 100 kHz.

Supplementary Figures and Tables

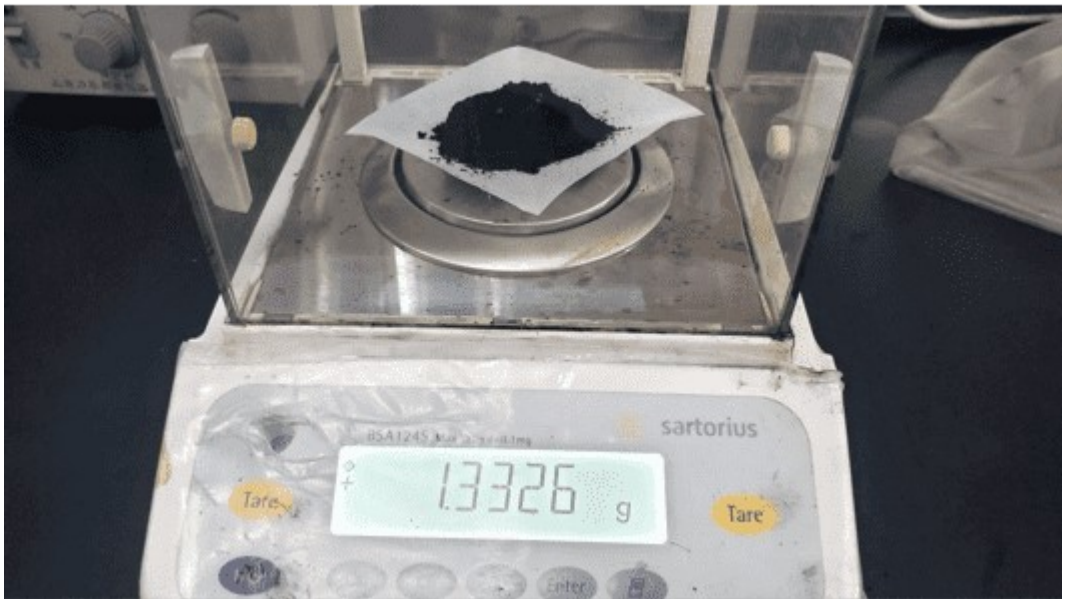

Figure S1. Photograph of catalyst yield after increasing the amount of reactants.

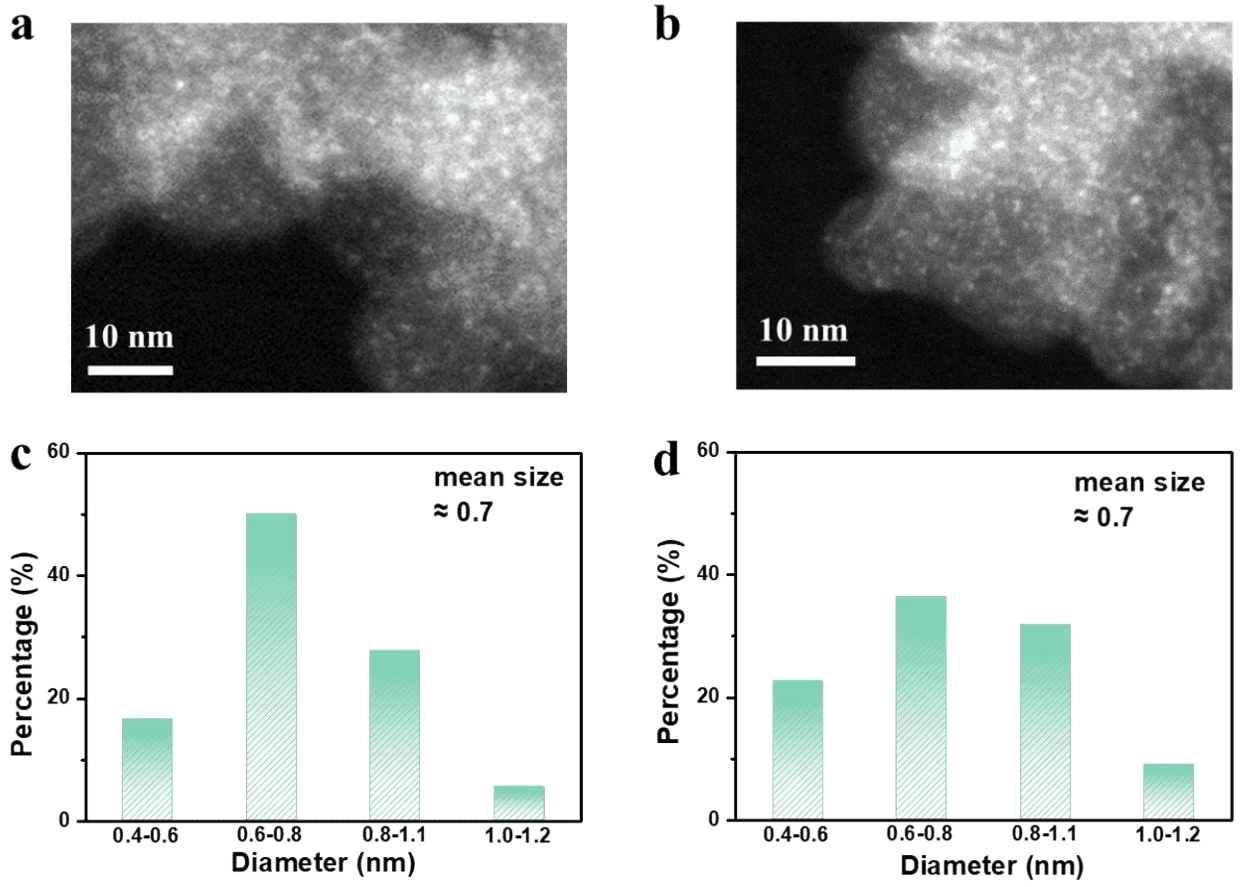

Figure S2. (a), (b) HAADF-STEM images for the $Pt_{0.6}$/KB-O_{S5}-40 at other regions and (c), (d) corresponding size distributions for the $Pt_{0.6}$/KB-O_{S5}-40.

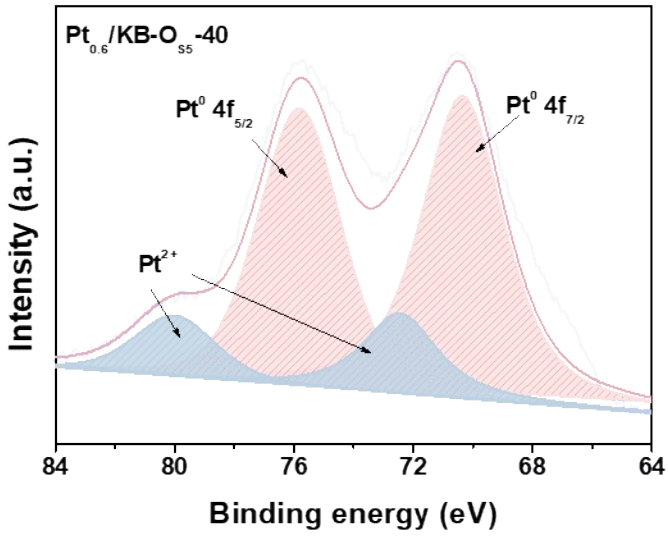

Figure S3. High-resolution Pt 4f XPS spectrum for $Pt_{0.6}$/KB-O_{S5}-40.

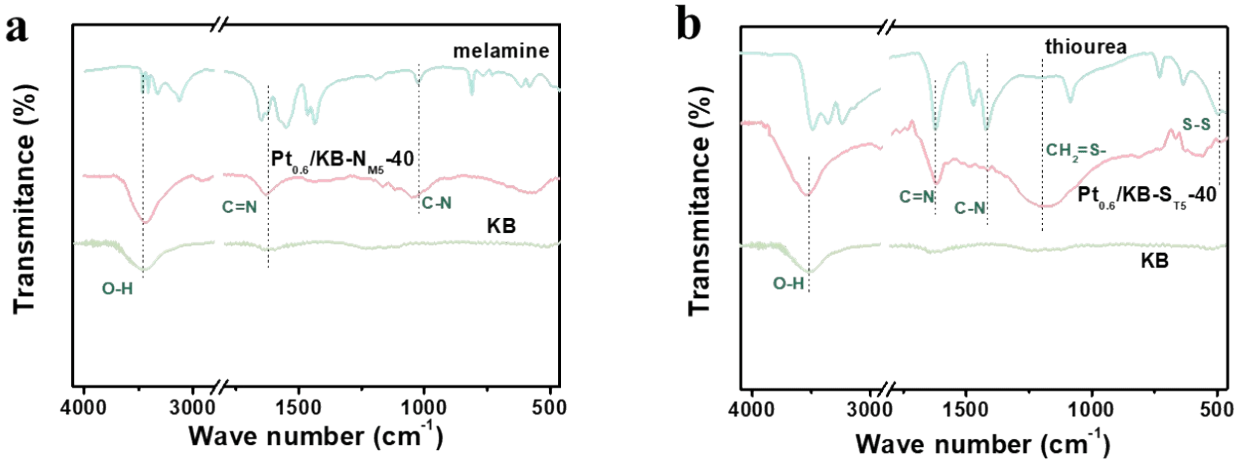

Figure S4. FTIR spectra of (a) $Pt_{0.6}$/KB-N_{M5}-40 and (b) $Pt_{0.6}$/KB-S_{T5}-40.

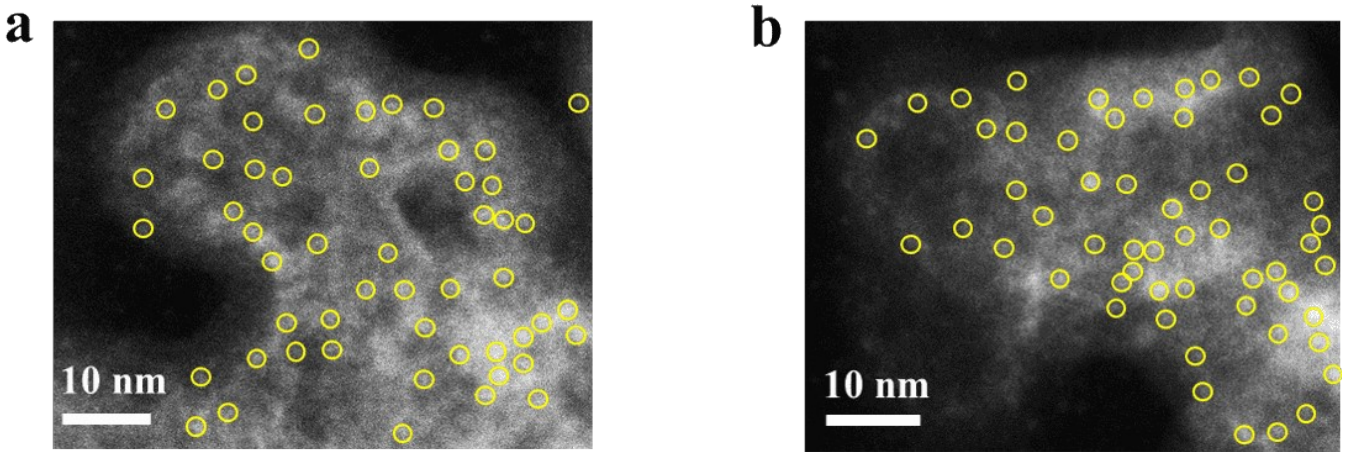

Figure S5. HRTEM images of (a) $Pt_{0.6}$/KB-N_{M5}-40 and (b) $Pt_{0.6}$/KB-S_{T5}-40.

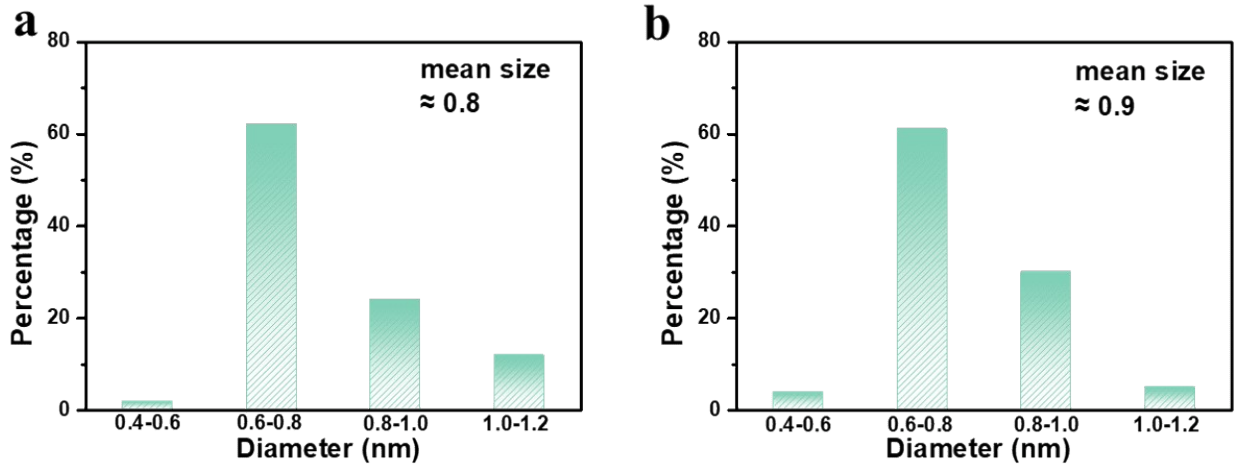

Figure S6. Corresponding size distributions for the (c) $Pt_{0.6}$/KB-N_{M5}-40 and (d) $Pt_{0.6}$/KB-S_{T5}-40.

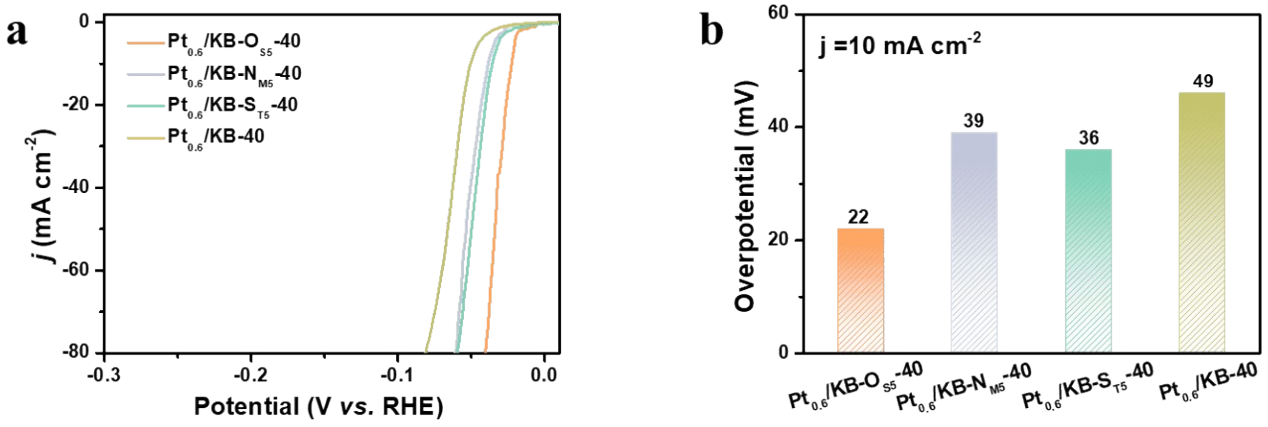

Figure S7. (a) LSV curves of $Pt_{0.6}$/KB-O_{S5}-40, $Pt_{0.6}$/KB-N_{M5}-40, $Pt_{0.6}$/KB-S_{T5}-40 and $Pt_{0.6}$/KB-40 in a N_2-saturated 0.5 M H_2SO_4. (b) Comparison η_{10} of $Pt_{0.6}$/KB-O_{S5}-40, $Pt_{0.6}$/KB-N_{M5}-40, $Pt_{0.6}$/KB-S_{T5}-40 and $Pt_{0.6}$/KB-40.

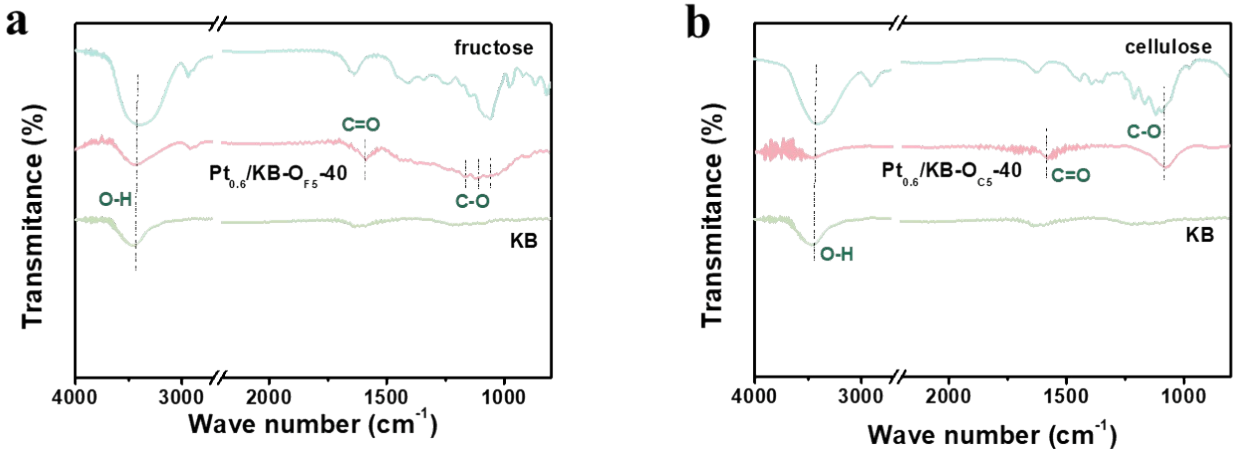

Figure S8. FTIR spectra of (a) $Pt_{0.6}$/KB-O_{F5}-40 and (b) $Pt_{0.6}$/KB-O_{C5}-40.

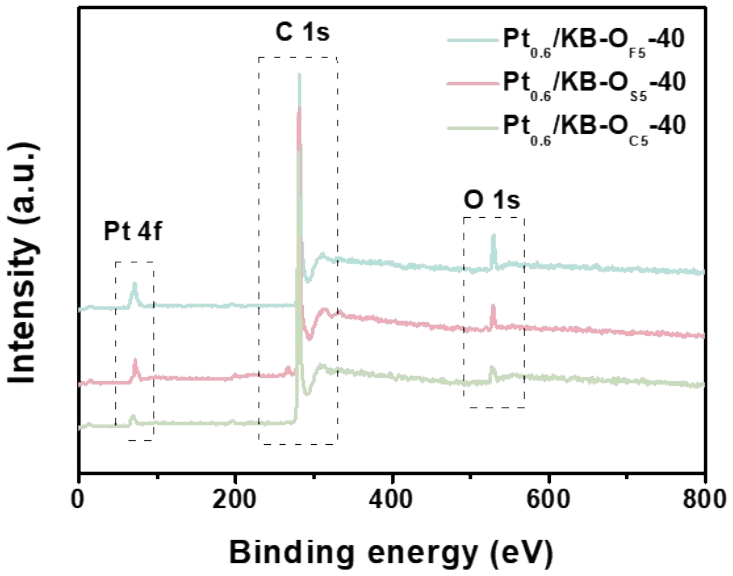

Figure S9. XPS spectra of $Pt_{0.6}$/KB-O_{F5}-40, $Pt_{0.6}$/KB-O_{F5}-40 and $Pt_{0.6}$/KB-O_{C5}-40.

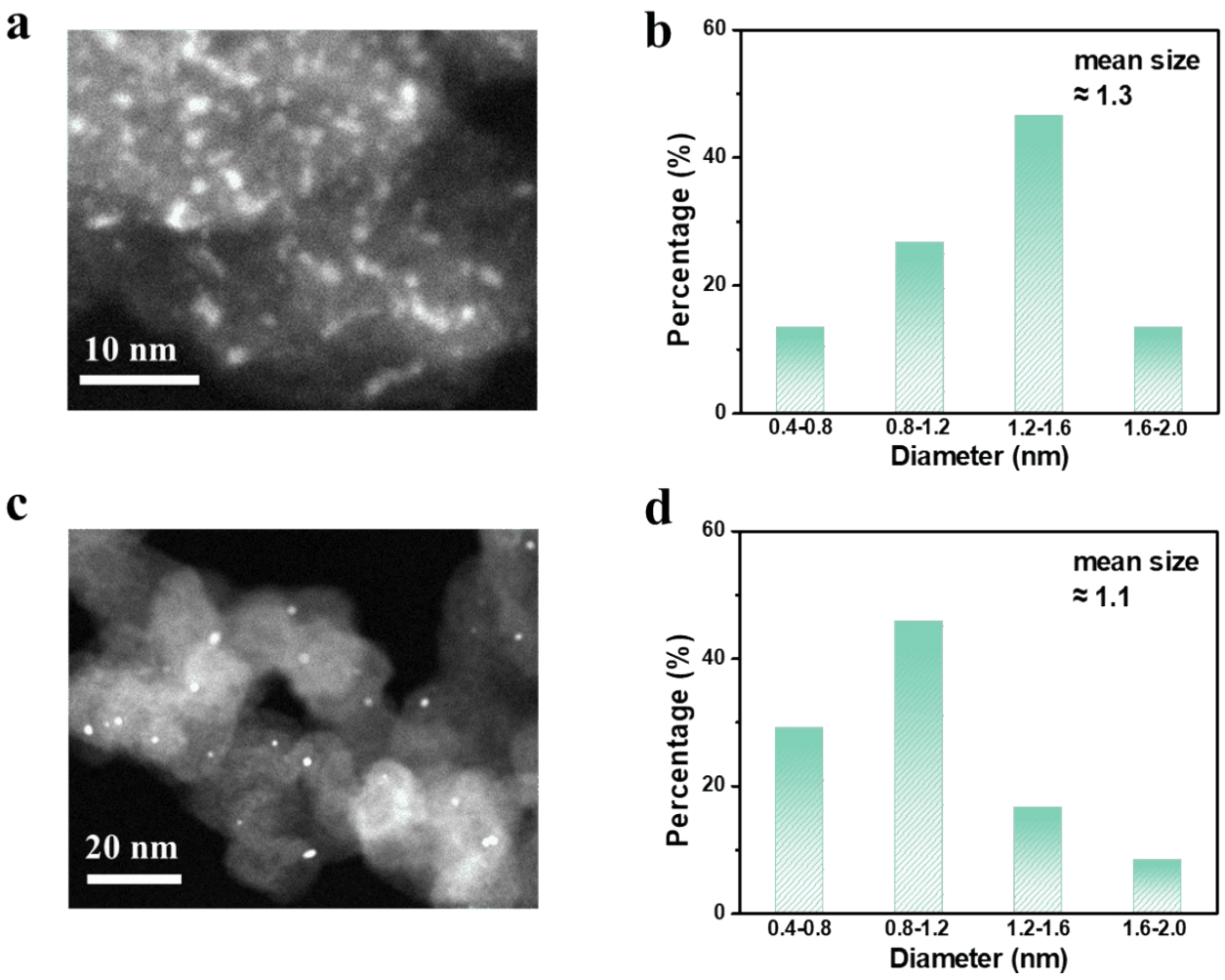

Figure S10. (a) HAADF-STEM image and (b) corresponding size distributions for $Pt_{0.6}$/KB-O_{F5}-40. (c) HAADF-STEM image and (d) corresponding size distributions for $Pt_{0.6}$/KB-O_{C5}-40.

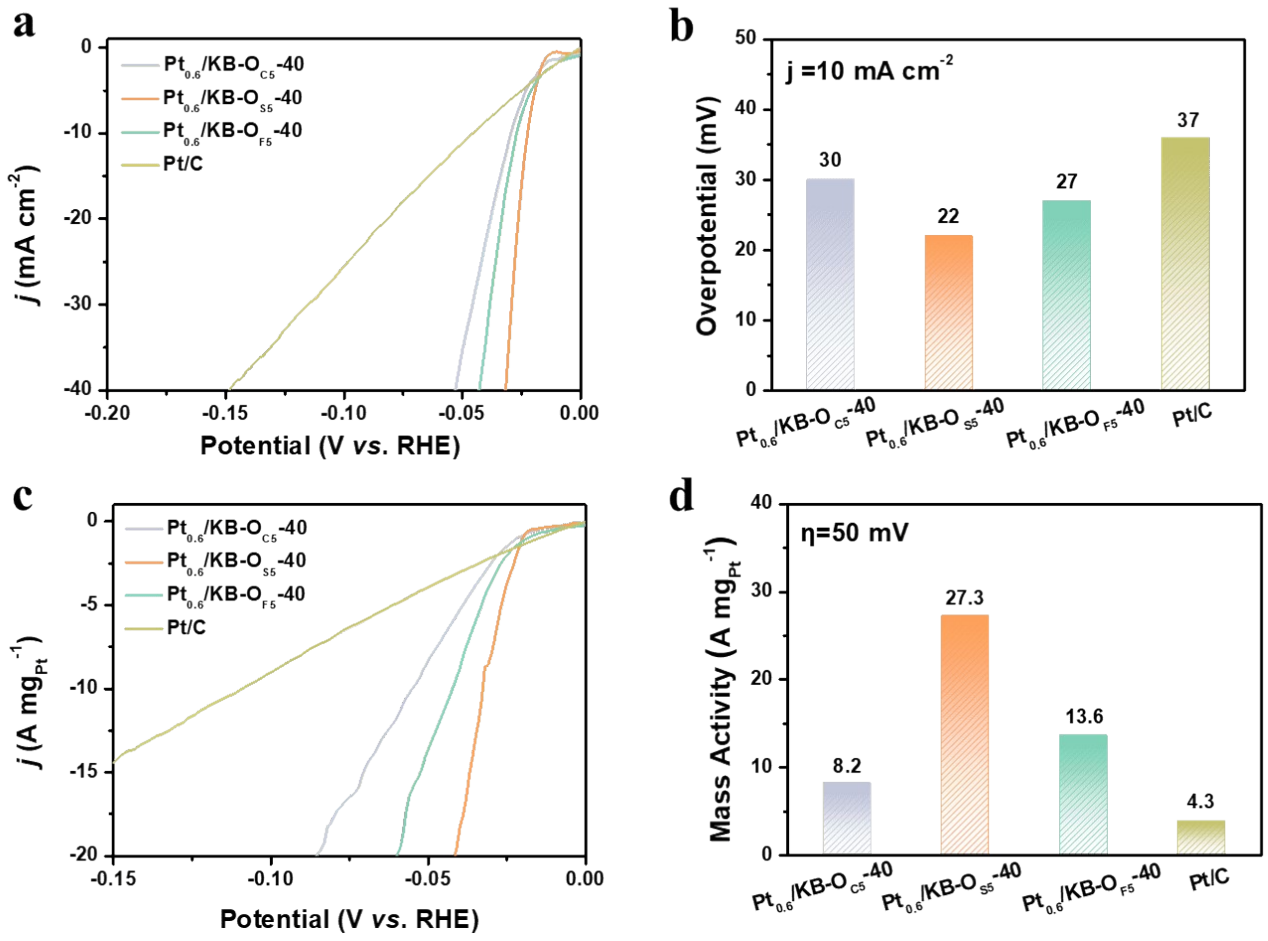

Figure S11. (a) LSV curves of $Pt_{0.6}$/KB-O_{C5}-40, $Pt_{0.6}$/KB-O_{S5}-40, $Pt_{0.6}$/KB-O_{F5}-40 and commercial Pt/C in a N_2-saturated 0.5 M H_2SO_4. (b) Comparison η_{10} of $Pt_{0.6}$/KB-O_{C5}-40, $Pt_{0.6}$/KB-O_{S5}-40, $Pt_{0.6}$/KB-O_{F5}-40 and commercial Pt/C. (c) LSV curves with the current density normalized to the Pt mass. (d) The mass activity of $Pt_{0.6}$/KB-O_{C5}-40, $Pt_{0.6}$/KB-O_{S5}-40, $Pt_{0.6}$/KB-O_{F5}-40 and commercial Pt/C at the overpotential of 50 mV.

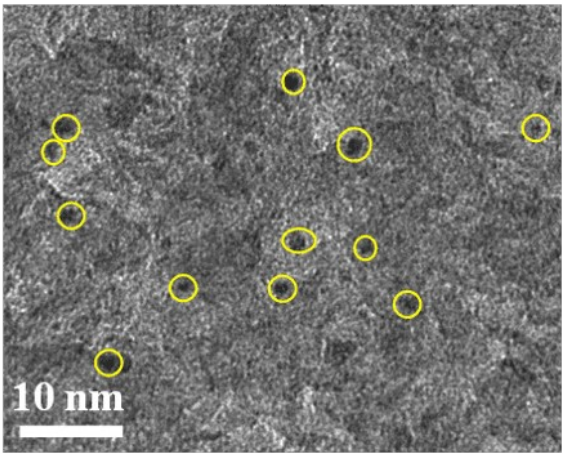

Figure S12. HRTEM image of $Pt_{0.6}$/KB-O_{S20}-40.

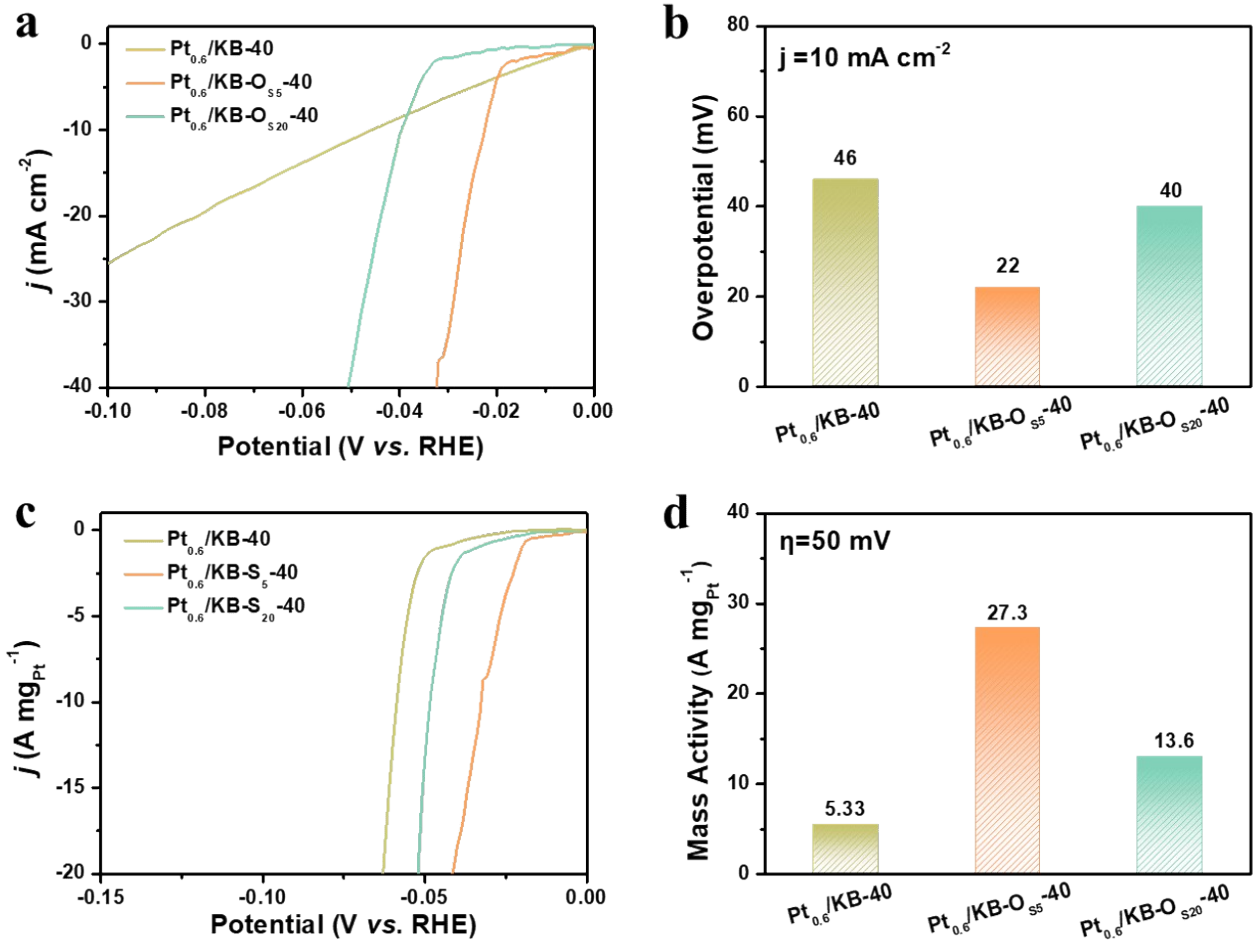

Figure S13. (a) LSV curves of $Pt_{0.6}$/KB-40, $Pt_{0.6}$/KB-O_{S5}-40 and $Pt_{0.6}$/KB-O_{S20}-40 in 0.5 M H_2SO_4. (b) Comparison η_{10} of $Pt_{0.6}$/KB-40, $Pt_{0.6}$/KB-O_{S5}-40 and $Pt_{0.6}$/KB-O_{S20}-40. (c) LSV curves of the HER with the current density normalized to the Pt mass. (d) The mass activity of $Pt_{0.6}$/KB-40, $Pt_{0.6}$/KB-O_{S5}-40 and $Pt_{0.6}$/KB-O_{S20}-40 when the overpotential is 50 mV.

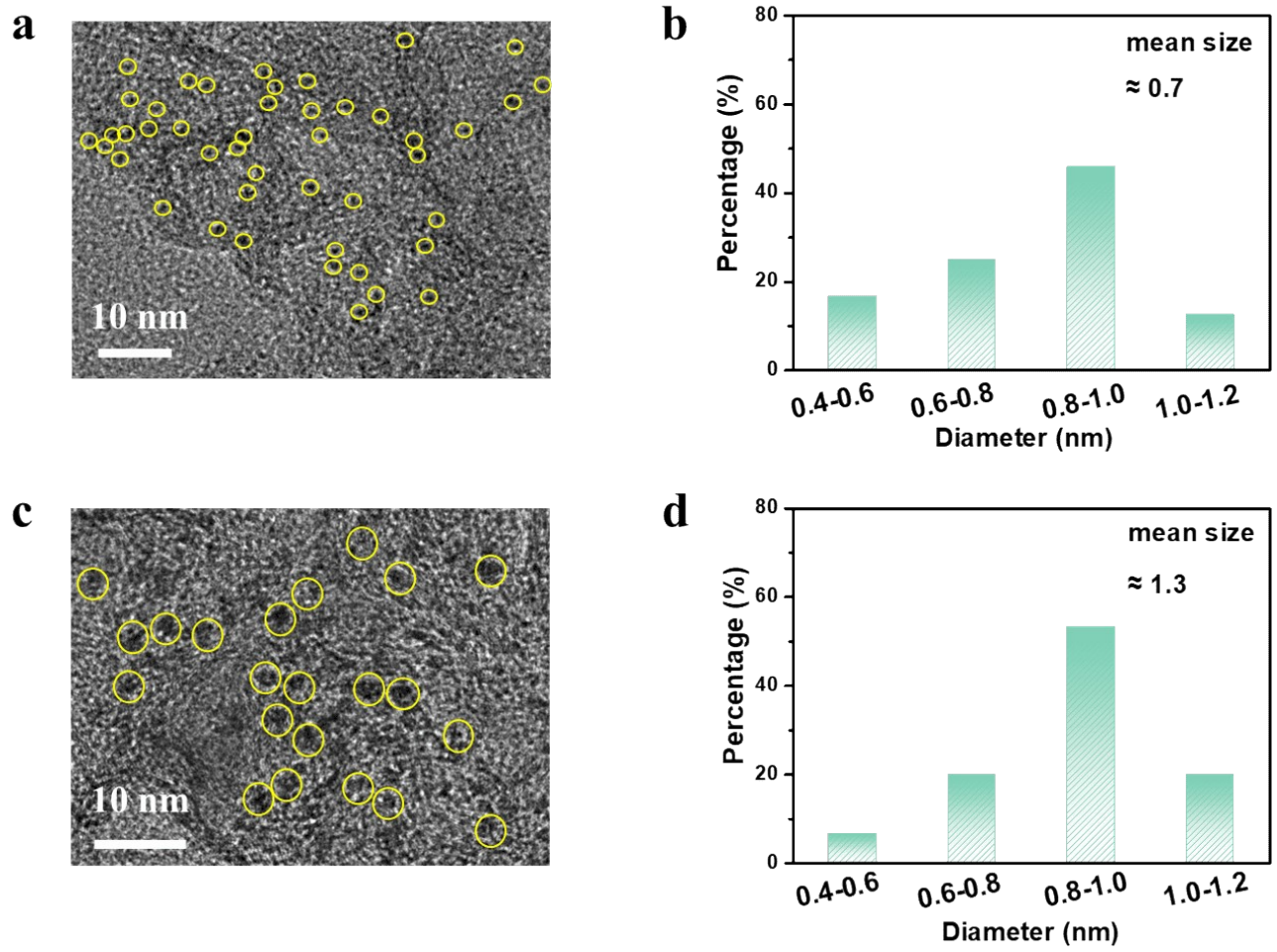

Figure S14. (a) HRTEM and (b) corresponding size distributions for $Pt_{0.6}$/KB-O_{S5}-20. (c) HRTEM and (d) corresponding size corresponding size distributions for $Pt_{0.6}$/KB-O_{S5}-60.

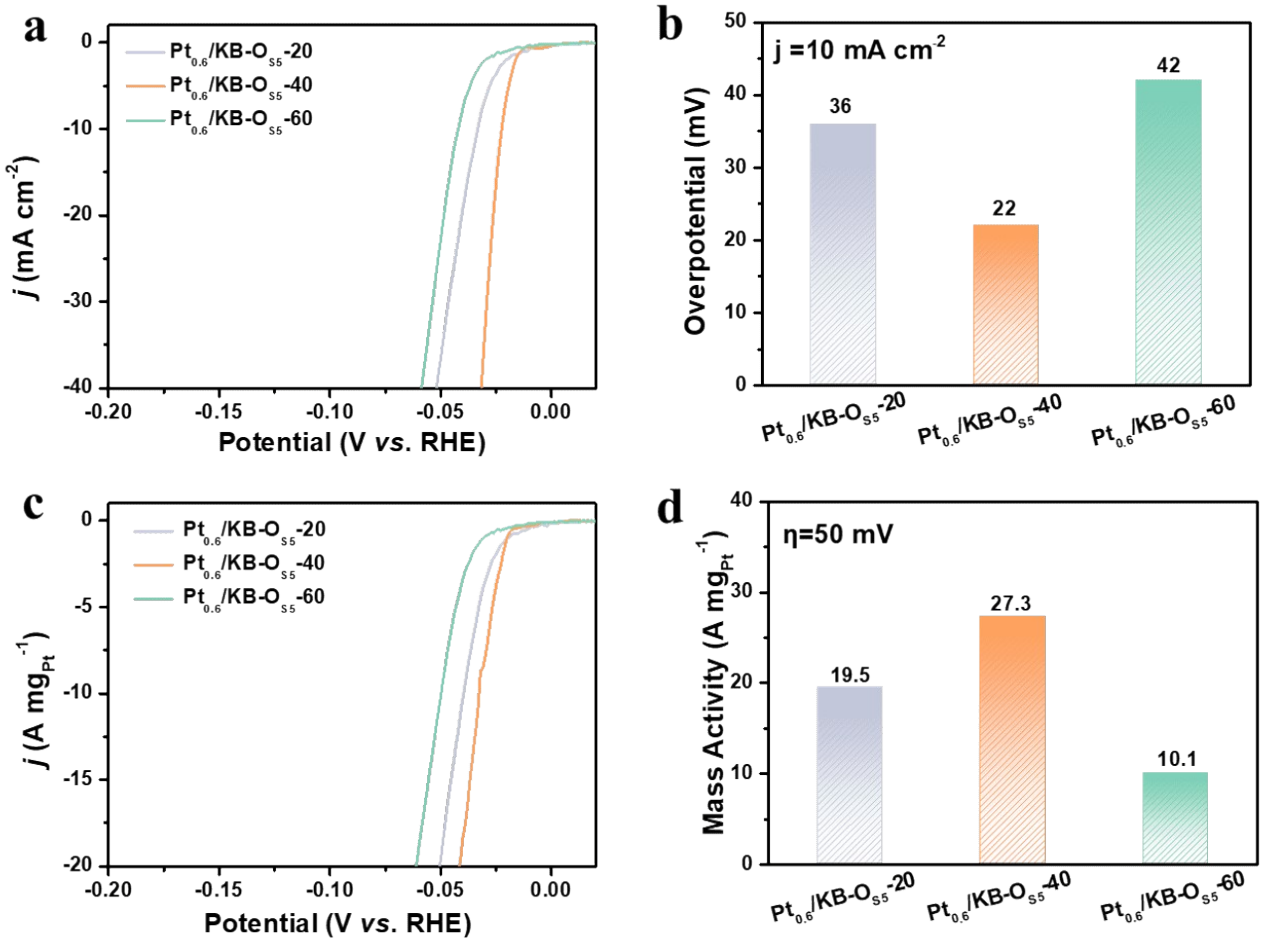

Figure S15. (a) LSV curves of $Pt_{0.6}$/KB-O_{S5}-20, $Pt_{0.6}$/KB-O_{S5}-40 and $Pt_{0.6}$/KB-O_{S5}-60 in a N_2-saturated in 0.5 M H_2SO_4. (b) Comparison η_{10} of $Pt_{0.6}$/KB-O_{S5}-20, $Pt_{0.6}$/KB-O_{S5}-40 and $Pt_{0.6}$/KB-O_{S5}-60. (c) LSV curves of the HER with the current density normalized to the Pt mass. (d) The mass activity of $Pt_{0.6}$/KB-O_{S5}-20, $Pt_{0.6}$/KB-O_{S5}-40 and $Pt_{0.6}$/KB-O_{S5}-60 when the overpotential is 50 mV.

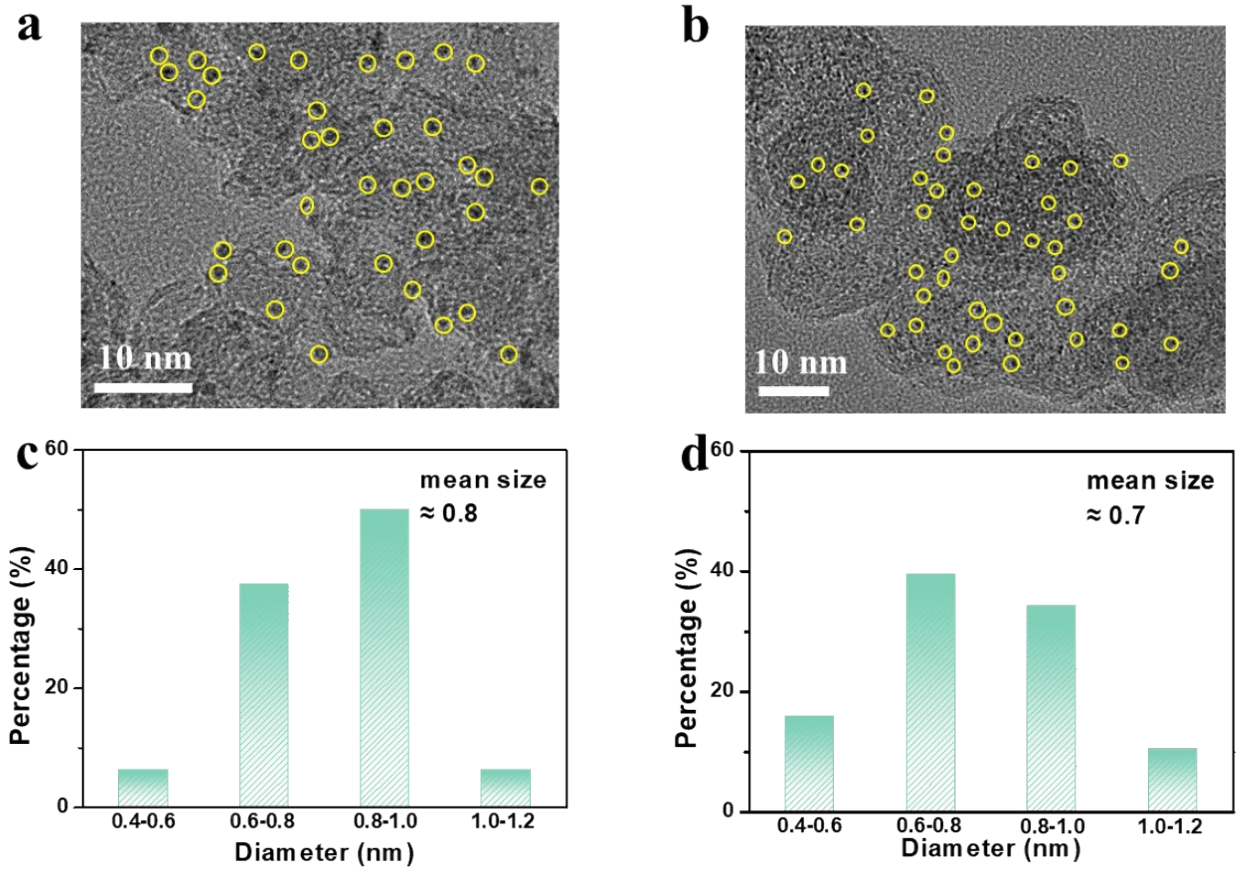

Figure S16. The HRTEM images of (a) $Pd_{0.6}$/KB-O_{S5}-40 and (b) $Ru_{0.6}$/KB-O_{S5}-40. Corresponding size distributions for the (c) $Pd_{0.6}$/KB-O_{S5}-40 and (d) $Ru_{0.6}$/KB-O_{S5}-40.

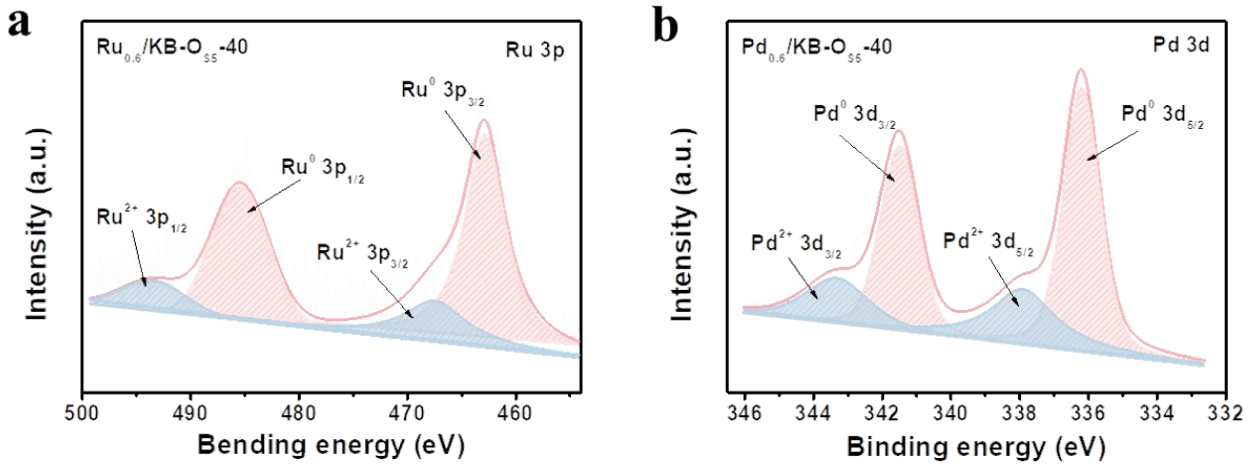

Figure S17. (a) High-resolution Ru 3p XPS spectrum for $Ru_{0.6}$/KB-O_{S5}-40. (b) High-resolution Pd 3d XPS spectrum for $Pd_{0.6}$/KB-O_{S5}-40.

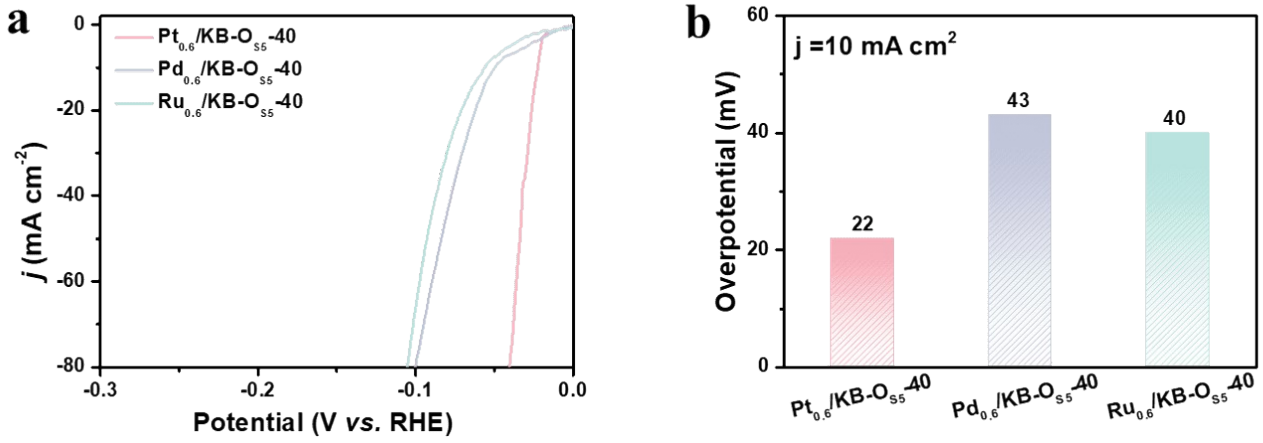

Figure S18. (a) LSV curves of $Pt_{0.6}$/KB-O_{S5}-40, $Pd_{0.6}$/KB-O_{S5}-40 and $Ru_{0.6}$/KB-O_{S5}-40 in 0.5 M H_2SO_4. (b) Comparison of η_{10} of $Pt_{0.6}$/KB-O_{S5}-40, $Pd_{0.6}$/KB-O_{S5}-40 and $Ru_{0.6}$/KB-O_{S5}-40.

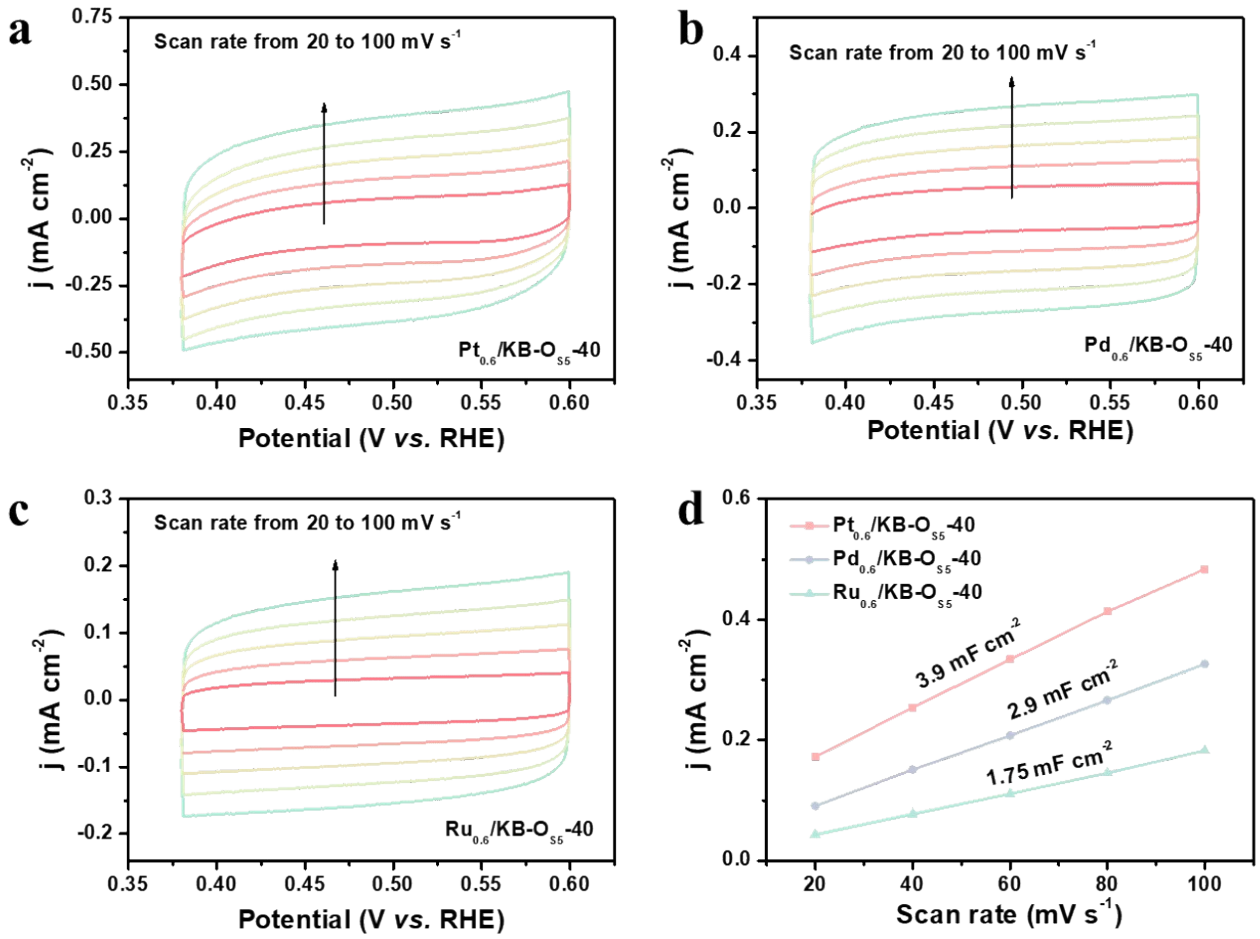

Figure S19. CV curves measured at different scan rates from 20 to 100 mV s^{-1} in 0.5 M H_2SO_4 for (a) $Pt_{0.6}$/KB-O_{S5}-40, (b) $Pd_{0.6}$/KB-O_{S5}-40 and (c) $Ru_{0.6}$/KB-O_{S5}-40. (d) Capacitive current at middle potential of CV curves as function of scan rates for $Pt_{0.6}$/KB-O_{S5}-40, $Pd_{0.6}$/KB-O_{S5}-40 and $Ru_{0.6}$/KB-O_{S5}-40.

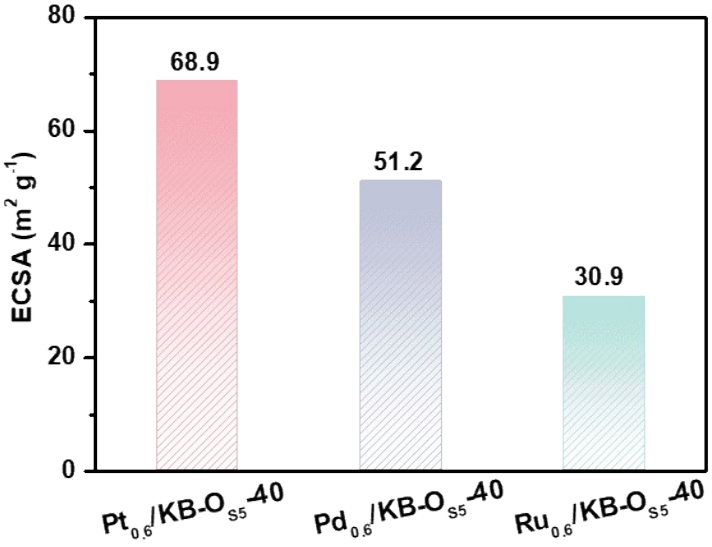

Figure S20. Estimation of the ECSA of $Pt_{0.6}$/KB-O_{S5}-40, $Pd_{0.6}$/KB-O_{S5}-40 and $Ru_{0.6}$/KB-O_{S5}-40.

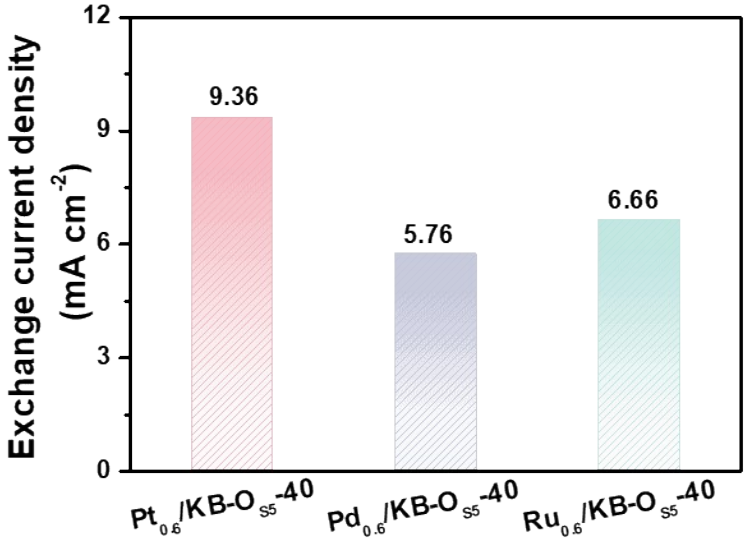

Figure S21. Exchange current density of $Pt_{0.6}$/KB-O_{S5}-40, $Pd_{0.6}$/KB-O_{S5}-40 and $Ru_{0.6}$/KB-O_{S5}-40.

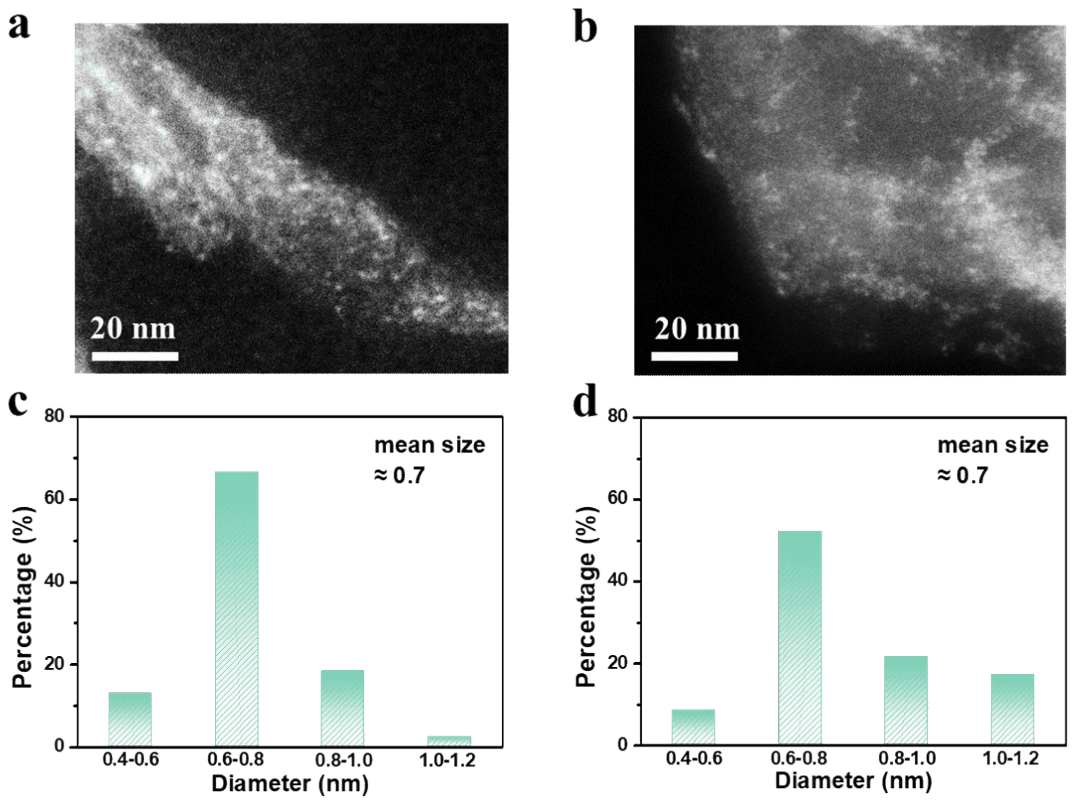

Figure S22. The HAADF-STEM images of (a) $Pt_{0.6}$/CNT-O_{S5}-40 and (b) $Pt_{0.6}$/rGO-O_{S5}-40. Corresponding size distributions for the (c) $Pt_{0.6}$/CNT-O_{S5}-40 and (d) $Pt_{0.6}$/rGO-O_{S5}-40.

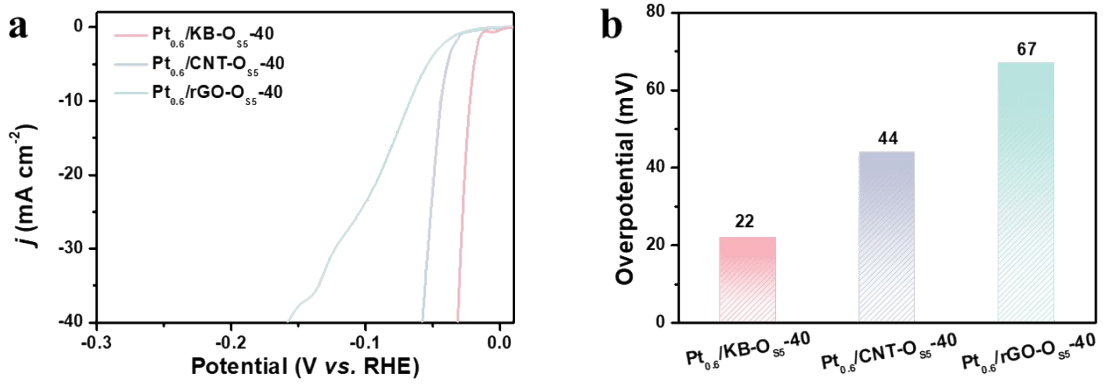

Figure S23. (a) LSV curves of $Pt_{0.6}$/CNT-O_{S5}-40, $Pt_{0.6}$/KB-O_{S5}-40 and $Pt_{0.6}$/rGO-O_{S5}-40 in 0.5 M H_2SO_4. (b) Comparison of η_{10} of $Pt_{0.6}$/CNT-O_{S5}-40, $Pt_{0.6}$/KB-O_{S5}-40 and $Pt_{0.6}$/rGO-O_{S5}-40.

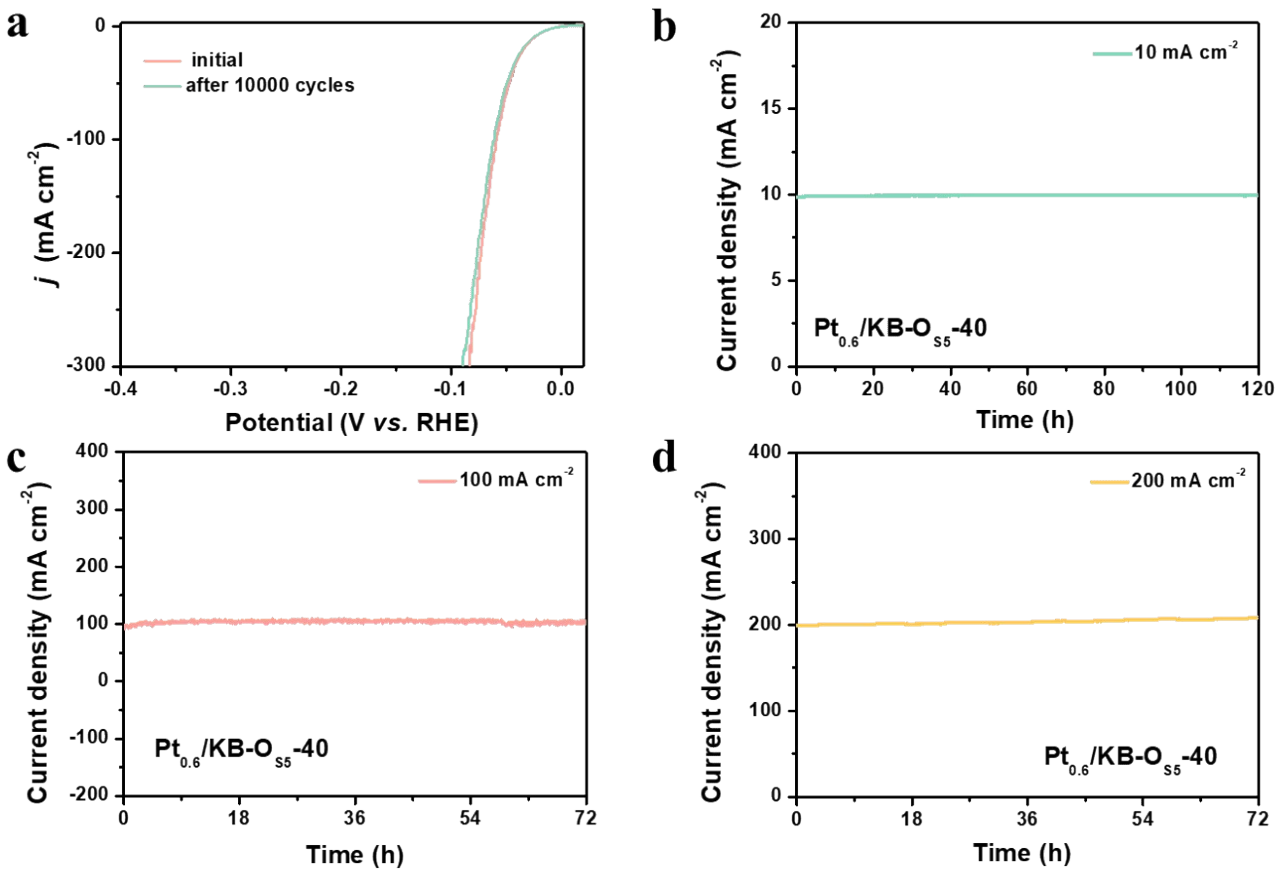

Figure S24. (a) LSV of HER of $Pt_{0.6}$/KB-O_{S5}-40 before and after 10,000 CV cycles. The current-time (i-t) curve of $Pt_{0.6}$/KB-O_{S5}-40 under the temporal evolution of the potential required to maintain (b)10 mA cm^{-2}, (c) 100 mA cm^{-2} and (d) 200 mA cm^{-2}.

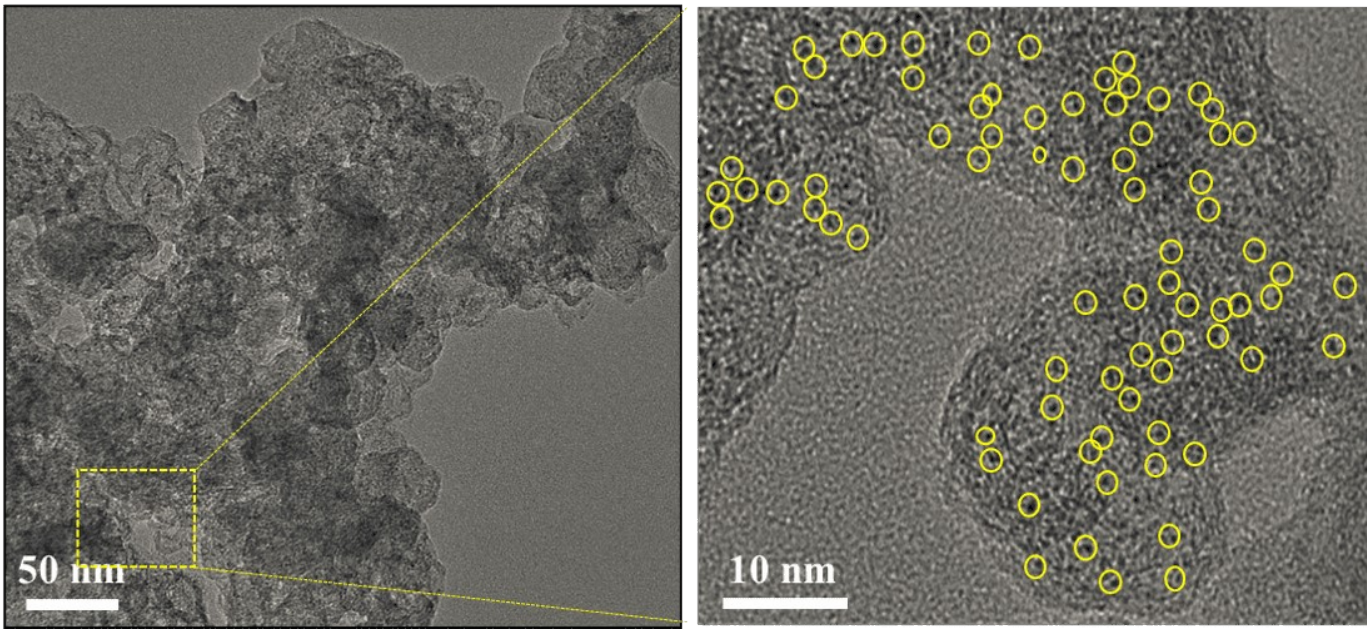

Figure S25. The HRTEM images of $Pt_{0.6}$/KB-O_{S5}-40 after ADT test in 0.5 M H_2SO_4.

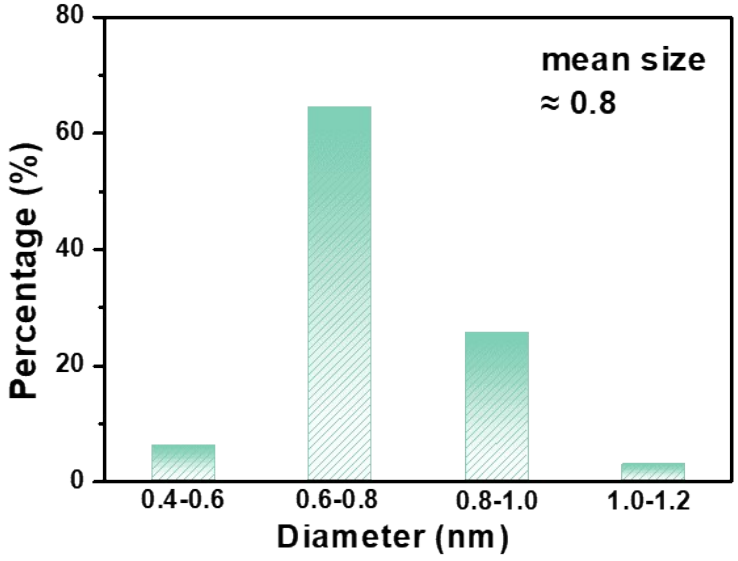

Figure S26. Corresponding size distributions for the $Pt_{0.6}$/KB-O_{S5}-40 after ADT test.

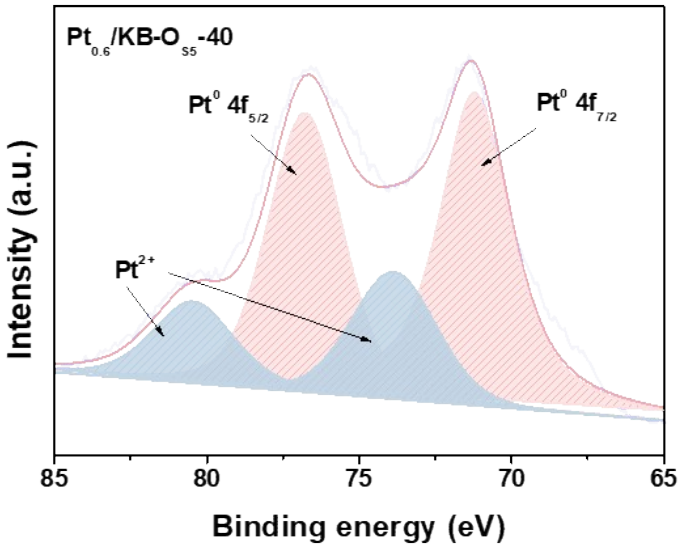

Figure S27. High-resolution Pt 4f XPS spectrum for $Pt_{0.6}$/KB-O_{S5}-40 after stability test.

Table S1. Mass fraction of different Pt/KB-S.

Material	*Metal loading (wt%)*
$Pt_{0.6}$/KB-O_{S5}-40	47.1
$Pt_{0.4}$/KB-O_{S5}-40	28.2
$Pt_{0.8}$/KB-O_{S5}-40	48.2
$Pt_{0.6}$/KB-O_{S5}-20	28.5
$Pt_{0.6}$/KB-O_{S5}-60	40.0
$Pt_{0.6}$/KB-40	12.3
$Pt_{0.6}$/KB-O_{S20}-40	49.8

Table S2. Metal loading of different functional groups, noble metals and carbon supports.

Material	*Metal loading (wt%)*
$Pt_{0.6}$/KB-N_{M5}-40	33.2
$Pt_{0.6}$/KB-S_{T5}-40	35.7
$Pt_{0.6}$/KB-O_{F5}-40	36.2
$Pt_{0.6}$/KB-O_{C5}-40	29.6
$Pd_{0.6}$/KB-O_{S5}-40	38.9
$Ru_{0.6}$/KB-O_{S5}-40	41.5
$Pt_{0.6}$/CNT-O_{S5}-40	40.7
$Pt_{0.6}$/rGO-O_{S5}-40	41.8

Table S3. HER performance of $Pt_{0.6}$/KB-O_{S5}-40 and other reported Pt-based catalysts in acidic medium.

Samples	***Overpotential (mV@ mA cm^{-2})***	***Pt loading (wt%)***	***Mass activity (A/mg@ overpotential)***	***Tafel slope (mV dec^{-1})***	***References***
$Pt_{0.6}$/KB-O_{S5}-40	22@10	47.1%	27.3@50 mV	21.9	this work
Pt-AC/DG	41@10	1.0%	15.6@50 mV	28	1
Pt/SWCNT-400	27@10	19.4%	1.1@50 mV	38	2
Pt_1/hNCNC	15@10	0.3%	7.6@20 mV	28	3
Pt_1/NPC	25@10	0.3%	2.9@25 mV	28	4
Pt/CNTs-ECR	34@10	0.2%	65@50 mV	26	5
Pt_1/MoO_{3-x}/C	23@10	2.0%	3.5@25 mV	28	6
PtCoFe@CN	45@10	1.3%	1.4@50mV	---	7
ALD_{50}Pt/NGNs	41@10	1.6%	10.1@50 mV	---	8
Pt@NHPCP	57@10	0.2%	5.0@50 mV	---	9
PtO_x/TiO_2	---	1.4%	15@50 mV	31	10
Pt@PCM	19@10	0.1%	---	63.7	11
$Mo_2TiC_2T_x$-Pt_{SA}	15@10	2.4%	1.3@10 mV	30	12
Pt-graphdiyne	66@100	0.9%	2.3@100 mV	47	13
PtO_x/TiO_2	---	1.4%	8.7@50 mV	40	10
MoS_2@Pt	70@10	3.4%	4.1@10 mV	36	14
Pt_1/MoO_{3-x}/C	23@10	4.1%	---	29	6
Pt-MoS_2	53@10	5.3%	2.0@10 mV	40	15
WC@C@Pt	30@10	13.9%	0.4@10 mV	26	16
Pt-CNSs/rGO	75@10	15.8%	0.9@10 mV	29	17
PtNiCu	25@10	10.7%	0.5@10 mV	28	18
$Pt_{66}Ni_{34}$ nanoflowers	43@10	4.0%	0.3@10 mV	33	19
Pt/MoS_2	86@10	1.3%	1.3@10 mV	52	20
$Pt_{2.6}Co_1$ nanoflowers	40@10	15.0%	0.3@10 mV	42	21

References:

1. Q. Cheng, C. Hu, G. Wang, Z. Zou, H. Yang and L. Dai, Carbon-defect-driven electroless deposition of Pt atomic clusters for highly efficient hydrogen evolution, *J. Am. Chem. Soc.*, 2020, **142**, 5594-5601.
2. M. Tavakkoli, N. Holmberg, R. Kronberg, H. Jiang, J. Sainio, E. I. Kauppinen, Tanja Kallio and K. Laasonen, Electrochemical activation of single-walled carbon nanotubes with pseudo-atomic-scale platinum for the hydrogen evolution reaction, *ACS Catal.*, 2017, **7**, 3121-3130.
3. Z. Zhang, Y. Chen, L. Zhou, C. Chen, Z. Han, B. Zhang, Q. Wu, L. Yang, L. Du, Y. Bu, P. Wang, X. Wang, H. Yang and Z. Hu, The simplest construction of single-site catalysts by the synergism of micropore trapping and nitrogen anchoring, *Nat. Commun.*, 2019, **10**, 1657.
4. T. Li, J. Liu, Y. Song and F. Wang, Photochemical solid-phase synthesis of platinum single atoms on nitrogen-doped carbon with high loading as bifunctional catalysts for hydrogen evolution and oxygen reduction reactions., *ACS Catal.*, 2018, **8**, 8450-8458.
5. X. Bao, Y. Gong, Y. Chen, H. Zhang, Z. Wang, S. Mao, L. Xie, Z. Jiang and Y. Wang, Carbon vacancy defect-activated Pt cluster for hydrogen generation, *J. Mater. Chem. A*, 2019, **7**, 15364-15370.
6. W. Liu, Q. Xu, P. Yan, J. Chen, Y. Du, S. Chu and J. Wang, Fabrication of a single-atom platinum catalyst for the hydrogen evolution reaction: A new protocol by utilization of H_xMoO_{3-x} with plasmon resonance, *ChemCatChem*, 2018, **10**, 946-950.
7. J. Chen, Y. Yang, J. Su, P. Jiang, G. Xia and Q. Chen, Enhanced activity for hydrogen evolution reaction over CoFe catalysts by alloying with small amount of Pt, *ACS Appl. Mater. Interfaces.*, 2017, **9**, 3596-3601.
8. N. Cheng, S. Stambula, D. Wang, M. N. Banis, J. Liu, A. Riese, B. Xiao, R. Li, T. K. Sham, L. M. Liu, G. A. Botton and X. Sun, Platinum single-atom and cluster catalysis of the hydrogen evolution reaction, *Nat. Commun.*, 2016, **7**, 13638.
9. J. Ying, G. Jiang, Z. P. Cano, L. Han, X. Yang and Z. Chen, Nitrogen-doped hollow porous carbon polyhedrons embedded with highly dispersed Pt nanoparticles as a highly efficient and stable hydrogen evolution electrocatalyst, *Nano Energy*, 2017, **40**, 88-94.
10. C. Xing, Y. Li, L. Zheng, Y. Yan, Y. Zhang, G. Chen, S. Sun and J. Zhang, Highly active, stable oxidized platinum clusters aselectrocatalysts for the hydrogen evolutionreaction., *Energy Environ. Sci.*, 2017, **10**, 2450-2458.
11. H. Zhang, P. An, W. Zhou, B. Y. Guan, P. Zhang, J. Dong and X. W. D. Lou, Dynamic traction of lattice-confined platinum atomsinto mesoporous carbon matrix for hydrogenevolution reaction., *Sci. Adv.*, 2018, **4**, eaao6657.
12. J. Zhang, Y. Zhao, X. Guo, C. Chen, C.-L. Dong, R.-S. Liu, C.-P. Han, Y. Li, Y. Gogotsi and G. Wang, Single platinum atoms immobilized on an MXene as an efficient catalyst for the hydrogen evolution reaction, *Nat. Catal.*, 2018, **1**, 985-992.
13. X. Yin, H. Wang, S. Tang, X. Lu, S. Miao, R. Si and T. Lu, Engineering the coordination environment of single-atom Pt anchored on graphdiyne for optimizing electrocatalytic hydrogen evolution, *Angew. Chem. Int. Ed.*, 2018, **57**, 9382-9386.
14. X. Xu, X. F. Dong, Z. J. Bao, R. Wang, J. G. Hu and H. B. Zeng, Three electron channels toward two

types of active sites in MoS_2@Pt nanosheets for hydrogen evolution, *J. Mater. Chem. A*, 2017, **5**, 22654-22661.
15. X. Huang, Z. Zeng, S. Bao, M. Wang, X. Qi, Z. Fan and H. Zhang, Solution-phase epitaxial growth of noble metal nanostructures on dispersible single-layer molybdenum disulfide nanosheets, *Nat. Commun.*, 2013, **4**, 1444.
16. Z. Liu, X. Huo, K. Xi, P. Li, L. Yue, M. Huang, G. Suo, L. Xu, W. Wang and X. Qu, Thickness controllable and mass produced WC@C@Pt hybrid for efficient hydrogen production., *Energy Storage Mater.*, 2018, **10**, 268-274.
17. G. Xu, J. Hui, T. Huang, Y. Chen and J. Lee, Platinum nanocuboids supported on reduced graphene oxide as efficient electrocatalyst for the hydrogen evolution reaction, *J. Power Sources*, 2015, **285**, 393-399.
18. C. Xia, Y. Han, C. Gao, Y. Xu, H. Xiaomin, M. Willander and N. Wang, Highly catalytic active PtNiCu nanochains for hydrogen evolution reaction, *Nano Energy*, 2014, **9**, 301-308.
19. X. Huang, X. Zhu, X. Zhang, L. Zhang, J. Feng and A. Wang, Simple solvothermal synthesis of uniform $Pt_{66}Ni_{34}$ nanoflowers as advanced electrocatalyst to significantly boost the catalytic activity and durability of hydrogen evolution reaction, *Electrochim. Acta*, 2018, **271**, 397-405.
20. W. Ren, H. Zhang and C. Cheng, Ultrafine Pt nanoparticles decorated MoS_2 nanosheets with significantly improved hydrogen evolution activity, *Electrochim. Acta*, 2017, **241**, 316-322.
21. L. Jiang, X. Lin, A. Wang, J. Yuan, J. Feng and X. Li, Facile solvothermal synthesis of monodisperse $Pt_{2.6}Co_1$ nanoflowers with enhanced electrocatalytic activity towards oxygen reduction and hydrogen evolution reactions, *Electrochim. Acta*, 2017, **225**, 525-523.